ELSEVIER

Cretaceous Research 26 (2005) 21–32

CRETACEOUS RESEARCH

www.elsevier.com/locate/CretRes

Upper Cretaceous oceanic red beds in southern Tibet: a major change from anoxic to oxic, deep-sea environments

Chengshan Wang[a,b], Xiumian Hu[c,*], Massimo Sarti[d], Robert W. Scott[e], Xianghui Li[a]

[a]*State Key Laboratory of Oil/Gas Geology and Exploitation, Chengdu University of Technology, Chengdu 610059, PR China*
[b]*China University of Geosciences, 29 Xueyuan Lu, Beijing 100083, PR China*
[c]*Department of Earth Sciences, Nanjing University, Nanjing 210093, PR China*
[d]*Department of Marine Science, Università Politecnica delle Marche, Ancona 60131, Italy*
[e]*Precision Stratigraphy Associates, RR3 Box 103-3, Cleveland, OK 74020, USA*

Accepted in revised form 15 November 2004
Available online 12 January 2005

Abstract

Red marine mudstones intercalated with pelagic marlstones, limestones and radiolarian cherts comprise the Chuangde Formation, which overlies mid-Cretaceous dark grey shales in the northern subzone of the Himalayan Tethys of southern Tibet. The red mudstones reflect deposition below the carbonate compensation depth (CCD) in a deep oceanic basin. The intercalated, thin-bedded marlstones represent fine-grained turbidites derived from the upper slope and transported into the adjacent deep basin. Planktonic foraminifera and nannofossils in the marlstones indicate a Santonian–early Campanian age for the formation. The red beds of the Chuangde Formation were deposited in a highly oxygenated deep-sea environment. This is confirmed by the high iron-trioxide content, the negative Cerium anomaly at the bottom of the red sequence, and the very low total organic carbon content (TOC 0.01–ca. 0.14%). Deposition of the red beds coincided with a Santonian–early Campanian diversity peak of planktonic foraminifera. The environmental interpretation is supported by the bulk carbon isotope $\delta^{13}C$ value of carbonate turbidites that becomes more positive stratigraphically up from the base of the formation. The highly oxygenated bottom-water conditions were not restricted to a deep ocean basin, but extended up to the continental rise/slope, as indicated by synsedimentary red marls incorporated in slumps and olistoliths near the top of the formation. This indicates that not only the bottom waters but also intermediate waters were highly oxygenated. Deposits of the Chuangde Formation are similar to Upper Cretaceous oceanic red beds (CORBs) in Western Europe, such as the Scaglia Rossa in Italy and the Capas Rojas in southern Spain. They represent the easternmost occurrence of Upper Cretaceous pelagic red beds of the Tethys. Late Cretaceous oxic oceanic conditions extended into the southern Tethys because the formation was deposited in southern palaeolatitudes. Therefore, the change from a dysoxic/anoxic to an oxic bottom ocean environment during the Late Cretaceous was at least hemiglobally if not globally wide. The change to oxic bottom conditions occurred later in the southern Tethys than in the western Tethys, where it began during the late Turonian. Several different earth processes could have caused such change. We suggest that the oxidized character of these deep-sea deposits was a result of a combination of various processes, among which very low sedimentation rates and changes in bottom ocean circulation may have been the most important.

Keywords: Oceanic/pelagic red beds; Late Cretaceous; Southern Tibet; Tethys; Dissolved oxygen

* Corresponding author.
E-mail address: huxm@nju.edu.cn (X. Hu).

0195-6671/$ - see front matter © 2005 Elsevier Ltd. All rights reserved.
doi:10.1016/j.cretres.2004.11.010

1. Introduction

Cretaceous "Oceanic Anoxic Events" (OAEs) (Schlanger and Jenkyns, 1976; Jenkyns, 1980; Scholle and Arthur, 1980) are associated with widespread deposition of organic carbon in deep-sea deposits (Schlanger et al., 1987), a major positive $\delta^{13}C$ excursion (Arthur et al., 1988; Jenkyns et al., 1994; Stoll and Schrag, 2000; Voigt, 2000) and marine biotic extinctions (Raup and Sepkoski, 1984; Kaiho, 1994a; Harries et al., 1996; Erbacher and Thurow, 1997; Harries, 1999; Leckie et al., 2002). However, much less attention has been given to the state of the oceanic environment in the aftermath of OAE2 when the deposition of organic carbon-enriched "black shale" facies was replaced by deposition of pelagic red beds (Jansa et al., 1979). A similar change in depositional environment was recorded during field work in southern Tibet (Fig. 1) where the underlying Coniacian dark grey shale of the Gyabula Formation is overlain by Santonian–Campanian pelagic red beds of the Chuangde Formation (Li et al., 1999; Wang et al., 2000).

This paper focuses on the study of the Upper Cretaceous oceanic red beds (CORBs) of the Chuangde Formation exposed in southern Tibet. Sedimentological, geochemical, and micropalaeontological data are used to compare the composition and stratigraphic position of the formation with similar deposits in Western Europe. In addition, geochemical and micropalaeontological data are used to test hypotheses of the process or processes that may have been responsible for such a major change in the redox conditions in the deep ocean.

2. Geological setting

Mesozoic sedimentary rocks are exposed in the Tethyan Himalayas between the Higher Himalayan Crystalline Belts and the Indus-Yarlung Zangbo Suture (Gansser, 1964; Burchfiel et al., 1992; Wang et al., 1996) (Fig. 1). During the mid-Cretaceous, this region was situated on the northern continental margin of the Indian Plate, approximately at a palaeolatitude of 20° S (Patzelt et al., 1996; Hay et al., 1999). The Mesozoic strata belong to two different tectonic domains: the passive continental margin of the Indian continental plate and the adjacent deep oceanic basin that separated the former from the Asian Plate (Yu and Wang, 1990; Liu and Einsele, 1994; Wang et al., 1996) (Fig. 1). The Gyirong-Kangmar intracrustal thrust subdivides the Tibetan Himalayas into the northern and southern tectonic subzones (Fig. 1). With the development of the Himalayan orogenesis as a result of the collision between the Indian and Eurasian plates, the Cretaceous sequence, together with other Mesozoic and Cenozoic marine strata on the northern margin of the Indian Plate, experienced strong tectonic deformation and thrusting. Outcrops of the sedimentary sequences are well exposed because there is little vegetation.

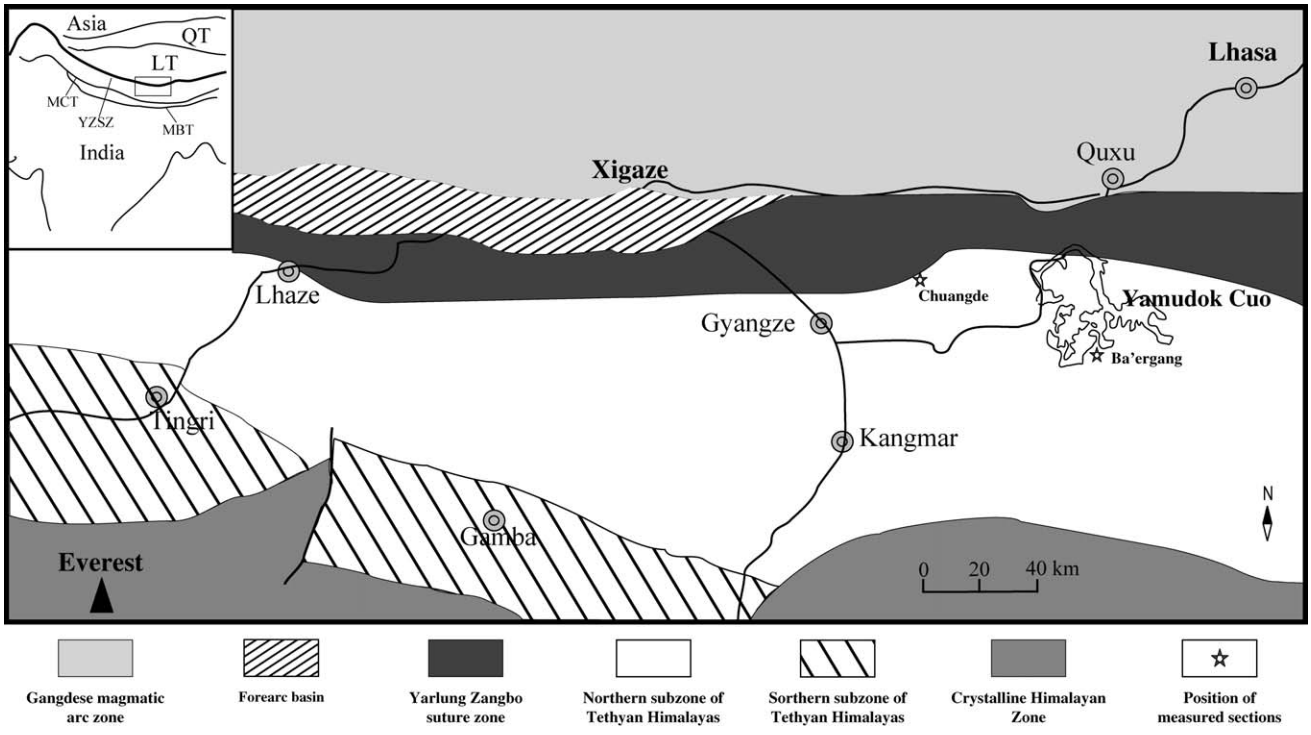

Fig. 1. Simplified geological map of the central part of southern Tibet showing tectonic situation and localities studied. QT, Qiangtang Terrane; LT, Lhasa Terrane; MCT, Main Central Thrust; MBT, Main Boundary Thrust; YZSZ, Yarlung Zangbo Suture Zone.

The stratigraphic framework in southern Tibet lacks the detailed biostratigraphic control that is available in the Alps and classical Cretaceous localities of Italy. However, work on Tibetan strata during recent decades has established a relatively detailed biostratigraphic scheme for the Cretaceous in the southern subzone of the Tibetan Himalayas (Inner Indian shelf zone of the Gamba-Tingri area; Fig. 1).

In the southern subzone, middle to Late Cretaceous sequences were deposited mainly on a passive shelf and upper continental slope (Yu and Wang, 1990; Willems, 1993; Liu and Einsele, 1994; Willems et al., 1996; Hu, 2002). Cretaceous strata in the northern subzone were deposited mainly on the deeper part of the margin and in the deep oceanic basin. The study presented herein is based on the Chuangde section in the northern subzone near the town of Gyangze and on the Ba'ergang section south of Yamudok Cuo (Fig. 1).

Li et al. (1999) and Wang et al. (2000) redefined the Cretaceous strata in the Gyangze area and subdivided the succession into three formations: Gyabula, Chuangde, and Zongzhuo (Fig. 2). The Gyabula Formation (150–300 m thick) is composed of black shale with pyrite nodules intercalated with sandstones deposited by turbidity currents. A Berriasian–Coniacian age for the formation is suggested by the occurrence of the radiolaria *Coccodiscus holmesi*, *Coccodiscus* sp., *Eucyriticium* sp., *Hemicryptocapsa* sp., *Pseudocaulophacus floresensis* and *Theocampe tina* (Wang et al., 2001). The overlying Chuangde Formation is about 30 m thick

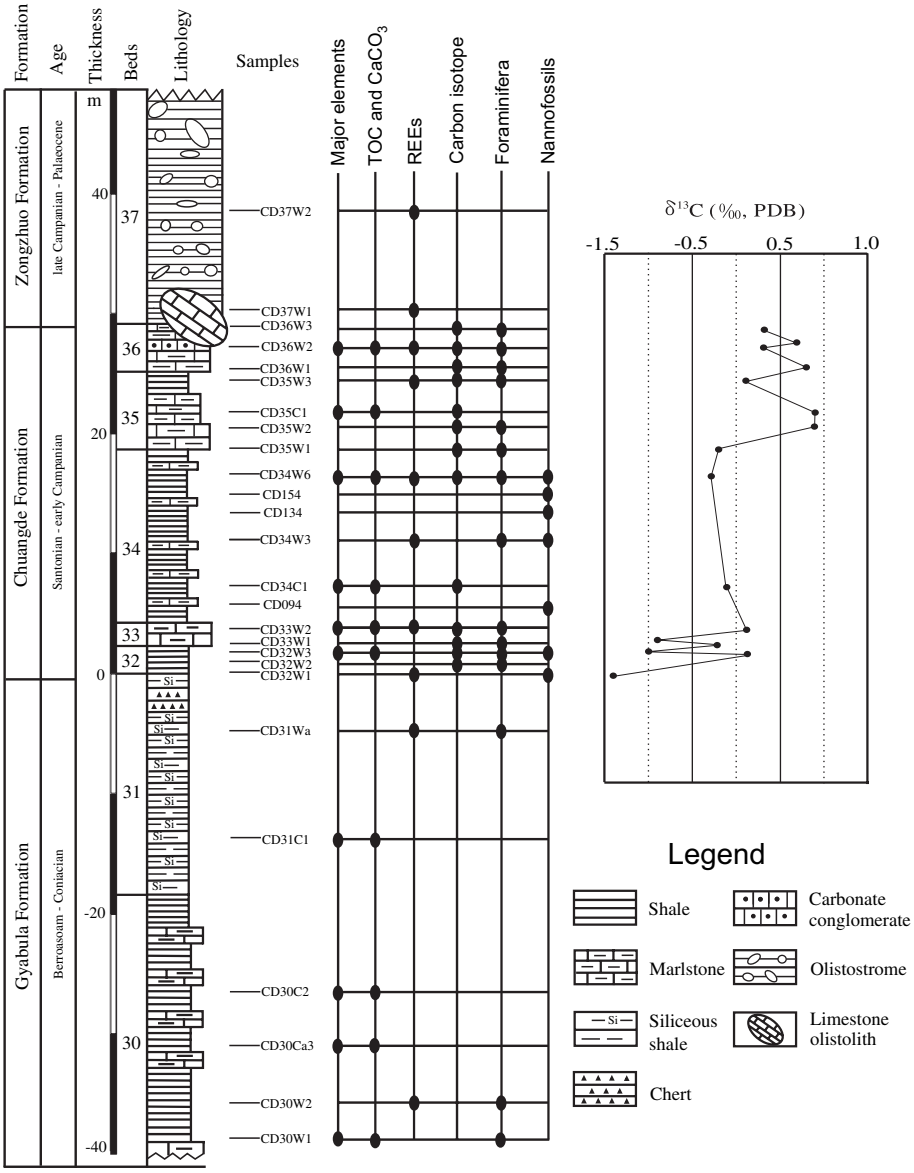

Fig. 2. Lithologic log showing sampling locations for the study of major elements, TOC and $CaCO_3$, REEs, carbon isotopes, foraminifera and nannofossils; also carbonate carbon isotope profile for the Chuangde section: PDB, Pee Dee Belemnite.

and consists of violet-red shales intercalated with thin marlstone beds. Foraminifera and nannofossils indicate a Santonian–early Campanian age for the formation (see below and Wan et al., 2005). The overlying Zongzhuo Formation is more than 200 m thick and of late Campanian–Palaeocene age (Liu and Aitchison, 2002). It is predominantly composed of dark grey to black shale enclosing various olistoliths of sandstone, limestone, and bedded chert that correspond to the "Beijia Olistostrome" of Liu and Einsele (1996).

In the Yamudok Cuo area, the Late Cretaceous red bed sequence is about 80 m thick and lithologically similar to that in the Gyangze area, except that it contains red radiolarian chert and several beds of carbonate and volcanic conglomerate debris flow deposits.

3. Methods

The sections studied in southern Tibet are well exposed, mostly on steep slopes largely devoid of scree. On the Tibetan Plateau, physical weathering dominates; chemical weathering is weak. The red colouration of the beds studied is primary and not a result of weathering or secondary oxidation, as demonstrated by the dark grey and greenish colours of the underlying and overlying beds. The field appearance of the Chuangde Formation is comparable to exposures of similar Late Cretaceous pelagic red beds, such as in the Carpathians and Austrian Alps.

Cenomanian–Campanian strata in southern Tibet were sampled at the Chuangde and Ba'ergang sections (Fig. 1), as noted above. Samples were collected from red beds of the Chuangde Formation at Chuangde at an interval of 0.2–0.5 m for sedimentology, micropalaeontology, geochemistry and carbon isotopes. Spacing outside the red bed interval was increased to 3–5 m per sample. At Ba'ergang the sample interval for biostratigraphy and sedimentology was 2–10 m. To avoid weathered rocks we took samples from trenches ca. 20 cm deep. Secondary oxidation of the underlying organic carbon-enriched beds of the Gyabula Formation did not penetrate beyond a depth of 5–10 cm.

Samples for foraminiferal study were broken down by repeated soaking and drying in 10% Na_2SO_4 solution, and were wet-sieved through a 0.5 mm mesh after several soaking/drying cycles. Residues were separated, dried, weighed, and size-sorted using sieves of 0.5, 0.25 and 0.16 mm mesh. Most planktonic foraminiferal tests encountered in thin sections are larger than 0.16 mm, but some are as small as 0.12 mm. Silt-sized tests are mostly composed of isolated broken chambers. All specimens were picked from each sieve size and mounted on slides. Counts of total numbers were compared to sample weights and expressed as number of specimens per 50 g.

Nannofossils from each sample were studied using standard methods of decantation, and smear slides were inspected under a light microscope (Zeiss Axiolab, magnification ×1500) and photographed.

Major oxides were analyzed by X-ray fluorescence spectrometry with instrumental precision for major elements within 1–2%. Rare earth elements (REEs), such as La, Ce, Nd, Sm, Eu, Tb, Yb, and Lu were analyzed in eight samples by Instrumental Neutron Activation Analysis (INAA) with a precision of 5–10% for La, Sm, Tb, Yb, and 10–15% for Ce, Nd, Eu, and Lu. Two samples were analyzed by Inductively Coupled Plasma-Atomic Emission Spectrography (ICP-AES) at the Yichang Institute of Geology and Mineral Resources. The lower limit of elemental analysis is ca.10^{-8}. Standard mean square deviation is 5–10%. The Cerium (δCe) and Europium anomalies (δEu) were calculated from (Ce sample/Ce shale)/Ce^* and (Eu sample/Eu shale)/Eu^*, where Ce^* and Eu^* are obtained by linear interpolation between shale-normalized La and Nd (Pr in ICP-AES), and Sm and Tb (Gd in ICP-AES) abundances, respectively. Normal shale values are from Piper (1974).

Samples for carbon isotope analysis of bulk carbonate were cleaned using 10% H_2O_2, then dried at 60 °C and subjected to phosphoric acid treatment at 90 °C. Isotope measurements of pure carbon dioxide were obtained on a Finnigan MAT 251 mass spectrometer at Chengdu University of Technology. The laboratory standard used in the measurements was calibrated relative to TTB-1 (China Laboratory Standard, Ordovician limestone in Zhoukoudian area, Beijing) and equals 0.58‰ for carbon relative to PDB (Pee Dee Belemnite). Normal corrections were applied and the results are reported in ‰ deviation from the PDB standard. Reproducibility error of replicate analyses of standards was less than 0.2‰. Diagenesis can adversely affect isotopic composition. In southern Tibet, light recrystallization and partial silicification suggest that Upper Cretaceous limestones experienced only low diagenetic transformation.

Total organic carbon (TOC) was determined on the CS-400 carbon-sulphur instrument at the Sichuan Institute of Oil and Gas Geology and Exploration. Determination of carbonate content was carried out by dissolving carbonate in powdered samples using concentrated CH_3COH and weighing the difference between the original and treated sample.

4. Results

4.1. Lithostratigraphy

In the Gyangze area, Turonian–Coniacian sediment composition changes from medium–dark grey and

grey-green shales of the Gyabula Formation to red shales of the Chuangde Formation (Fig. 3A). The latter are locally intercalated with thin marlstone beds (Fig. 2). The contact between the Gyabula and Chuangde formations is transitional (Fig. 3B). At the top of the Gyabula Formation, greenish grey-weathering shales are intercalated with thin siltstone beds and overlain by light grey-weathering, bioturbated, calcareous shales 20 m thick, which in fresh samples are dark grey. The shales are in sharp contact with an overlying bed of black radiolarian chert 0.5 m thick (Fig. 2), which in turn is overlain with a sharp contact by non-calcareous greenish shales 2.5 m thick that are intercalated by centimetre-thick beds of marlstone at 20–30-cm intervals. At the top of this basal shale unit is a 1-m-thick marlstone bed (Bed 33, Fig 2) that is intensively bioturbated and encloses pea- to small-pebble-sized greenish pods. The long axis of these pods is orientated parallel to the bedding plane. The pods are either intraclasts or faecal pellets. Above this marlstone bed the strata become largely brick red. They consist of non-calcareous, red shales with zones of intercalated, centimetre-thick, pink to red marlstone beds (Fig. 3C). The contact of the marlstones with the shales is sharp (Fig. 3C). The uppermost part of the Chuangde Formation is made up of thin-bedded, laterally discontinuous,

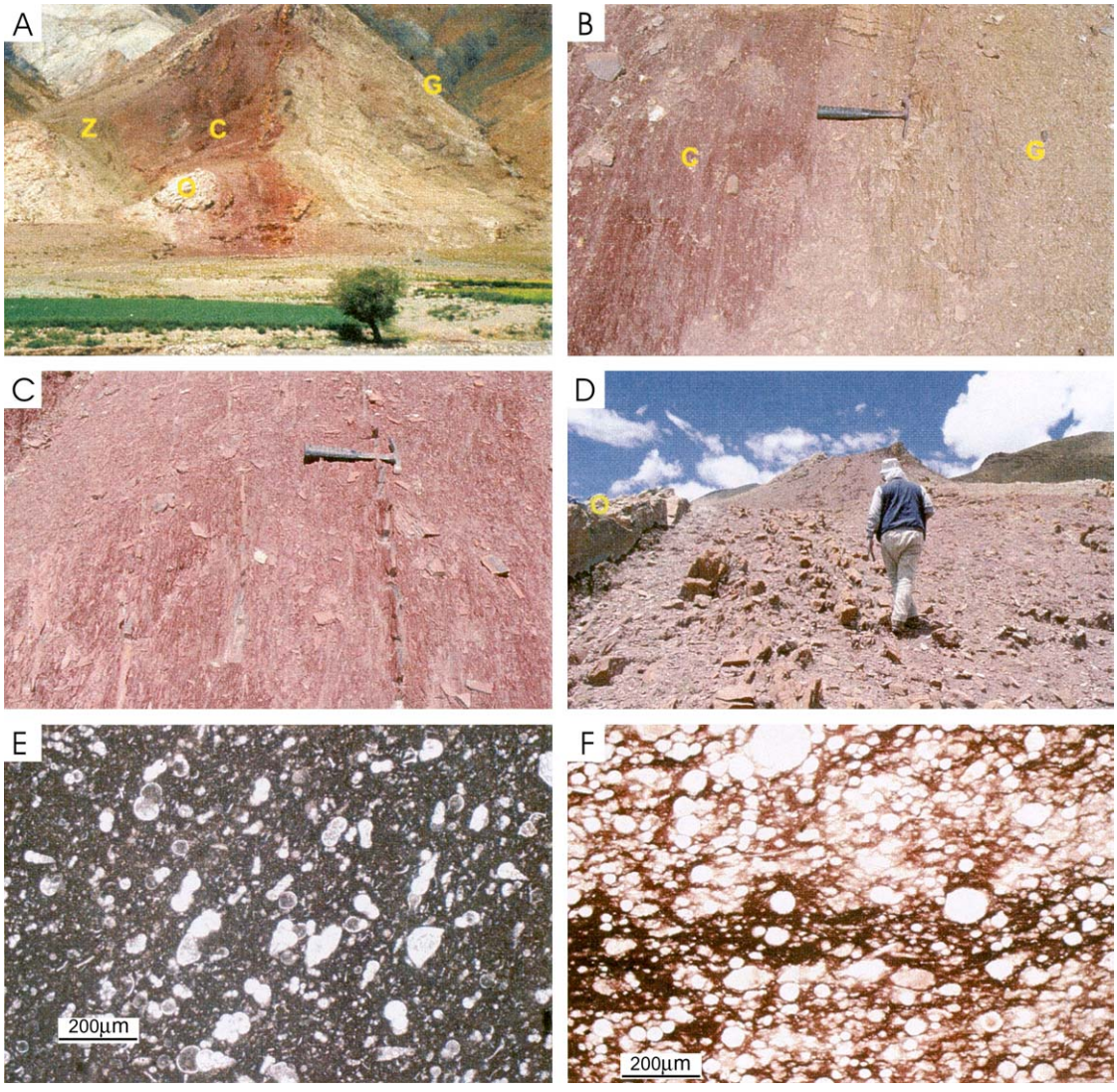

Fig. 3. A–E, field and thin section photographs of the red beds of the Chuangde Formation, Chuangde section. A, photograph of the section showing stratigraphic units: Gyabula Formation (G), light–dark grey shales; Chuangde Formation (C), interbedded red shales and marlstones; Zongzhuo Formation (Z), grey shales enclosing olistoliths (O); trees for scale. B, plan view of the transitional contact between the Gyabula (G) and Chuangde (C) formations; hammer for scale. C, plan view of the red shales intercalated with centimetre-thick bedded marlstones; hammer for scale. D, photograph showing discontinuous thin-bedded red marlstones; note the sharp contact between the marlstones and shales; person for scale. E, photomicrograph of the red marlstone, a planktonic foraminiferal wackestone; matrix stained by iron oxide; sample YL05. F, photomicrograph of red radiolarian chert; irregular laminae disrupted by bioturbation and heavy iron oxide stain; sample BG05, Ba'ergang section.

reddish marlstones (Fig. 3D) that are rich in planktonic foraminifera (Beds 35–36) and interbedded with red shales. Again, the contact between the marlstone and red shale is sharp. Near the top of the formation a thick-bedded, light-grey marlstone olistolith up to 10 × 30 m in size is overlain by 2 m of thin-bedded, red shales and limestones (Fig. 3A). The formation is overlain with a sharp contact by light greenish-grey, thin-bedded shales of the Zongzhuo Formation several tens of metres thick in which plastically deformed marlstone intraclasts up to 0.5 m in length are enclosed. The intraclasts show various slump features and contain contorted pieces of red shales. The rock texture and enclosed foraminiferal microfauna indicate that the marlstones represent periodic slumps from the upper part of the continental margin into the adjacent deep basin where the floor was below the CCD.

The red shales of the Chuangde Formation are composed of clay minerals stained by iron oxide (haematite), and trace amounts of very fine silt-sized quartz and mica. X-ray diffraction shows that illite is the dominant mineral in the clay fraction (30–90%) and chlorite is second in abundance (5–70%). Vermiculite, chlorite/vermiculite, and smectite-vermiculite random-mixed-layered structures are rare, and zeolites are lacking. Poorly preserved radiolarians, foraminifera, and unidentified rounded bodies similar to calcispheres are locally present in trace amounts. The marlstone beds are composed of nannomicrite with locally preserved nannofossils and variable amounts of planktonic foraminifera (Fig. 3E). Texturally, the marlstone laminae and thin beds range from mudstone to wackestone and even packstone. A bed of foraminiferal grainstone and a bed of limestone conglomerate are present near the top of the formation (Fig. 2). The rounded pebbles in the conglomerate consist of various clasts of foraminiferal wackestone, grainstone and lime mudstone, and rare inoceramid and calcareous sponge debris. The matrix between the pebbles is red clay.

In the Ba'ergang section the bedded, red radiolarian chert is bioturbated and intercalated with red shales. Chert texture ranges from packstone and wackestone to mudstone (Fig. 3F). Some of the radiolaria are diagenetically replaced by chalcedony, others by microsparite. The matrix of the chert consists of iron oxide (haematite), silica, and clay concentrated into thin, irregular laminae by dissolution.

4.2. Biostratigraphy

Planktonic foraminifers are abundant in the marlstones of the Chuangde Formation. The assemblage in the Chuangde section represents the *Dicarinella asymetrica* and *Globotruncanita elevata* zones of the Santonian and early Campanian (Caron, 1985; Robaszynski and Caron, 1995; Robaszynski in Hardenbol et al., 1998; Wan et al., 2005). It includes *Dicarinella asymetrica*, *D. concavata*, *Globotruncana lapparenti*, *G. linneiana*, *G. ventricosa*, *Globotruncanita elevata*, *G. stuartiformis*, *G.* sp., *Hedbergella* sp., *Heterohelix* sp., *Marginotruncana pseudolinneiana*, *M. schneegansi*, and *M. sinuosa*.

The Santonian–early Campanian age of the formation is also supported by nannofossils, although they are poorly preserved in the red beds. They include: *Biscutum* sp., *Calculites obscurus*, *Eiffellithus eximius*, *E. turriseiffelii*, *Eprolithus floralis*, *Gartnerago* sp., *Lucianorhabdus cayeuxii*, *Microrhabdulus decoratus*, *Micula decussata*, *Prediscosphaera cretacea*, *Quadrum gartneri*, *Reinhardtites anthophorus*, *Tranolithus phacelosus*, *Watznaueria barnesae* and *W. fossacincta*. Of these, *C. obscurus*, *L. cayeuxii* and *R. anthophorus* are stratigraphically important species for the Santonian (Perch-Nielsen, 1985; K. von Salis in Hardenbol et al., 1998). The first appearance datum (FAD) of *R. anthophorus* is the base of the CC15 Zone at 85.66 Ma (ages from Hardenbol et al., 1998, chart 5), and it ranges into the Campanian. The FAD of *L. cayeuxii* defines the base of the CC16 Zone, and that of *C. obscurus* at 84.32 Ma defines the base of the CC17 Zone, spanning the Santonian/Campanian boundary. The FAD of *Tranolithus* phacelosus is usually found in the lower Campanian (Perch-Nielsen, 1985). The presence of these nannofossil species indicates that the Chuangde Formation in the Chuangde section spans zones CC15–17 or younger, therefore including the Coniacian/Santonian boundary at 85.8 Ma to the early Campanian, which began at 83.5 Ma, hence a duration of more than 2.3 myr.

4.3. Major elements and REEs

Major element abundances in the red beds of the Chuangde Formation differ from those in the underlying dark grey shales of the Gyabula Formation (Table 1). The carbonate content in the latter is low, averaging 11.5%, and ranging from 0.9 to 33.3%. In the red shales above, $CaCO_3$ content averages 5.9% (14 samples), but increases up to 55–71% in the intercalated marlstone beds. Total organic carbon (TOC) content in the red beds is extremely low (0.01–ca. 0.14%), averaging 0.07% (8 samples). By contrast, TOC in the shales of the Gyabula Formation varies between 0.5 and 1.6%.

The red shales have higher Fe_2O_3 values, averaging 8.4% in weight, and a lower FeO content than the Gyabula shales. The enrichment in Fe_2O_3 of up to 10.2% in the red beds is attributed to deposition in an oxic environment where Fe^{2+} was oxidized to Fe^{3+}. At the base of the red beds the $Fe^{3+}/(Fe^{3+} + Fe^{2+})$ ratio abruptly increases from 0.51 to 0.99. Other elements such as MnO and total iron show no significant excursions at this stratigraphic level (Table 1).

Table 1
Comparison of selected trace elements from samples of the red limestones, Chuangde Formation and underlying Gyabula Formation, southern Tibet

Formation	Bed No.	Lithology		TOC%	$CaCO_3$%	S%	Mn^{2+}%	Sr%	FeO%	Fe_2O_3%
Chuangde Fm	32–36	Red limestone	Ranges	0.01–0.06	55–71	–	0.5–0.84	–	1.4–2.0	3.4–5.6
			Averages	0.03(3)	63(5)	–	0.67(2)	–	1.8(4)	4.3(4)
		Red shale	Ranges	0.01–0.14	0.5–30	0.024–0.038	0.12–0.14	0.007–0.034	0.9–3.9	3.9–10.2
			Averages	0.07(5)	5.9(14)	0.03(2)	0.13(5)	0.023(4)	1.8(14)	8.4(14)
Gyabula Fm	29–31	Grey shale	Ranges	0.5–1.0	0.9–33.3	0.01–0.04	0.09–0.37	0.008–0.019	0.5–4.5	1.4–5.4
			Averages	0.75(22)	11.5(12)	0.02(5)	0.22(6)	0.012(8)	2.5(10)	4.1(10)

Numbers in brackets indicate numbers of analyses.

Both the absolute concentrations of REEs and the shale-normalized patterns in the red beds differ from those of the overlying and underlying strata (Table 2; Fig. 4). The red marlstones are characterized by average REE values 32% higher than those of the Gyabula Formation (224×10^{-6} to ca. 281×10^{-6} compared to a range of 147×10^{-6} to ca. 230×10^{-6}) (Table 2). The high REE content of the red mudstone is attributed to increases in each rare earth element, with a 107% increase for Eu, 38–52% for La, Nd, Sm, Tb, Yb and Lu, and 17% for Ce. Compared with the other elements, Ce is relatively depleted. Shale-normalized patterns in the red marlstones have significantly larger excursions relative to other Cretaceous strata at the Chuangde locality, with a distinctively negative Ce-anomaly and a large positive Eu-anomaly (Fig. 4). Neither Ce nor Eu anomalies were found in the Gyabula or Zongzhuo formations. Corresponding to the appearance of the Chuangde red beds, δCe decreases from 0.96 to 0.66, which is a major change. It then increases gradually upwards to bed 35 (Fig. 4). δEu in the red beds increases gradually and reaches a maximum of 1.6 in bed 34, showing a strong positive anomaly (Fig. 4).

4.4. Carbon isotopes

Whole-rock carbon isotope values from carbonates in the red beds of the Chuangde Formation in the Chuangde section range from −1.4 to +0.9‰ $\delta^{13}C$, and become more positive towards the top of the formation (an average of 0‰ in 16 samples; Table 3, Fig. 2). $\delta^{13}C$ is much lower here than in the coeval marine carbonates in the shelf of the southern subzone near Tingri (an average of 1.9‰ in 14 samples; Hu et al., 2001). Because the carbonate beds within the Chuangde Formation represent turbidites derived from the adjacent continental slope, the carbon isotope data can be interpreted to indicate lower bioproductivity on the slope environment in comparison to the shelf areas.

5. Discussion

The colour of pelagic sediments is indication of redox conditions on the sea floor (Colley et al., 1984; Wilson et al., 1985; Thomson et al., 1987). The red colouring is a post-depositional feature and requires prolonged exposure of sediments to oxygen-rich bottom water (Thomson et al., 1987; Krenmayr, 1996; Eren and Kadir, 1999). This study confirms that the red colour of the Chuangde Formation is a result of the presence of disseminated haematite pigment, indicating oxidizing conditions near the sediment-water interface. The Fe_2O_3 values of the red beds are high, averaging 8.4% with a maximum of up to 10.2%. In the stratigraphic succession from non-red beds to red beds, the Fe^{3+}/

Table 2
Rare Earth Element (REE) concentrations in (ppm) and calculated parameters for the Chuangde section, southern Tibet

Fm	Sample	Lithology	La	Ce	Pr	Nd	Sm	Eu	Gd	Tb	Dy	Ho	Er	Tm	Yb	Lu	∑REE	δCe	δEu
Zongzhuo	CD37W3	Grey shale	31.5	62.1		42.2	6.3	1.1		0.9					3.1	0.4	147.4	0.8	0.9
	CD37W1	Grey shale	51.4	80.3		51.1	13.2	2.7		1.8					4.0	0.5	205.1	0.7	1.0
Chuangde	*CD36W2	Red marl	29.3	64.6	8.3	34.9	5.9	1.7	5.0	0.8	4.4	0.9	2.2	0.3	2.1	0.3	139.7	1.0	1.4
	CD35W3	Red marl	45.7	70.3		43.9	11.1	2.5		1.6					3.5	0.5	179.1	0.8	1.1
	CD34W6	Red shale	64.4	99.9		57.5	13.1	4.1		1.8					4.9	0.7	246.3	0.8	1.6
	CD34W3	Red shale	54.8	94.4		53.7	11.0	3.3		1.4					4.9	0.6	224.3	0.8	1.6
	*CD33W2	Red marl	21.5	40.1	5.5	27.7	4.2	1.2	3.8	0.7	3.1	0.6	1.5	0.2	1.7	0.3	97.4	0.9	1.3
	CD32W1	Red shale	71.3	103.1		77.5	17.3	3.8		2.0					5.4	0.8	281.2	0.7	1.2
Gyabula	CD31Wa	Grey shale	37.3	80.1		42.2	8.6	2.0		1.3					2.9	0.4	174.7	1.0	1.1
	CD30W2	Grey shale	50.5	116.9		46.8	9.5	1.5		1.0					3.6	0.5	230.3	1.1	0.9

Sample positions indicated in the reference sections (Figs. 2, 4).
1, ∑LREE = (La + Ce + Nd + Sm + Eu), ∑HREE = (Tb + Yb + Lu), ∑REE = (∑LREE + ∑HREE).
2, *CD36W2, CD33W2 were analyzed by ICP-AES. Other samples were analyzed by INAA.

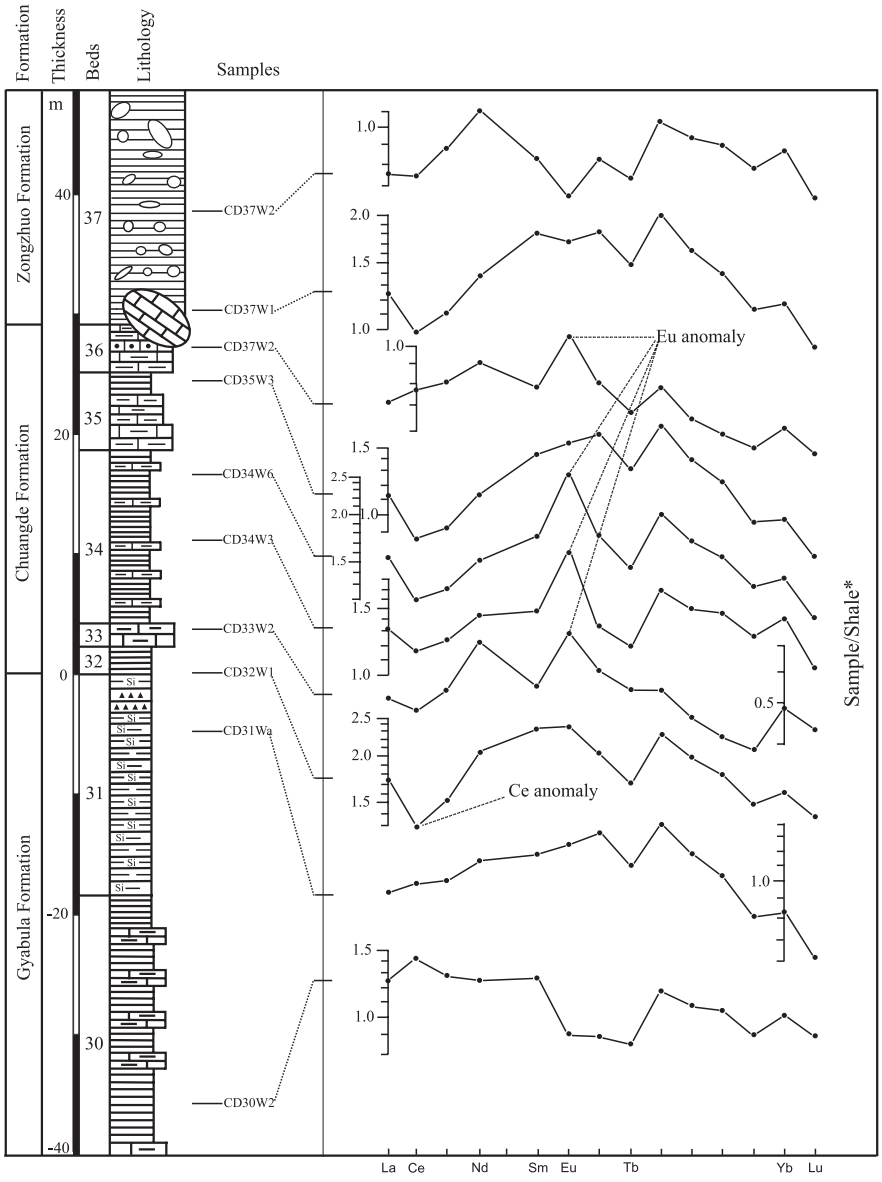

Fig. 4. Shale-normalized REE abundance patterns in the Chuangde section showing distinct excursions of Ce and Eu, with negative Ce-anomaly and positive Eu-anomaly. Normalized shale (shale*) is after Piper (1974).

($Fe^{3+} + Fe^{2+}$) ratio abruptly increases from 0.51 to 0.99. This change is interpreted to represent a redox change from a non-oxic to an oxic depositional environment. The oxic, deep-water environment of the red beds is further supported by a δCe anomaly. Studies of modern marine sediments demonstrate that sedimentary diagenesis can change the REE content but not its normalized pattern. Therefore, the decrease in δCe can be used to determine oxidizing–reducing conditions in sedimentary rocks (Shimizu and Masuda, 1977; Liu et al., 1988; Piper, 1994; Holser, 1997). The decrease of δCe from 0.96 to 0.66 in the basal part of the formation (Fig. 4) provides evidence for progressive change from a reducing to a highly oxidizing depositional environment. The very low TOC (0.01–0.14%) in the red shales could be either a result of low biogenic productivity or of highly oxygenated bottom waters, which in combination with a low sedimentation rate would allow deposited organic matter to be oxidized. However, a high dissolved-oxygen content in modern oceanic bottom waters (Morford and Emerson, 1999; Morford et al., 2001), such as in the northern North Atlantic, does not lead to the development of similar oxic, red clays; therefore, additional forcing factors were needed to deposit the red beds of the Chuangde Formation.

Using a very different approach from studies of calcareous benthic foraminiferal morphotypes, Kaiho (1994a,b) concluded that the highest oxygen levels in ocean-bottom waters occurred during the Santonian–Campanian. He used his data to propose oxygen index

Table 3
Carbon isotope data of bulk carbonate relative to PDB of the Chuangde Formation, Chuangde section, southern Tibet

Samples	Lithology	$\delta^{13}C$ (‰, PDB)
CD36W3	red marlstone	0.3
CD36.4	red marlstone	0.7
CD36W2	red marlstone	0.3
CD36W1	red marlstone	0.8
CD35W3	red marlstone	0.1
CD35C1	red marlstone	0.9
CD35W2	red marlstone	0.9
CD35W1	red marlstone	−0.2
CD34W6	red shale	−0.3
CD34C1	red shale	−0.1
CD33W2	red marlstone	0.1
CD33.1	red marlstone	−0.9
CD33W1	red marlstone	−0.2
CD32C1	red shale	−1.0
CD32W3	grey-green shale	0.1
CD32W2	red shale	−1.4

Sample positions are indicated in the reference section (Fig. 2).

curves for global mean values of intermediate and deep oceanic waters, and concluded that the dissolved oxygen level of the oceans has fluctuated throughout geologic time. The lowest oxygen levels since 100 Ma are associated with the Cenomanian/Turonian boundary (Schlanger and Jenkyns, 1976; Jenkyns, 1980) and the highest in the Santonian–Campanian (Kaiho, 1994a), which agrees with our data from southern Tibet. Oxygen content as interpreted by Kaiho (1994a,b) reflects conditions at the sediment-water interface and in the uppermost 10 cm of the sediment because the indices are derived from a study of epifauna and infauna (Kaiho, 1994a,b). Such information reflects early post-depositional (early diagenetic) conditions within deposited sediment and does not, therefore, provide a direct measure of the oxygen level in deep oceanic waters. According to Kaiho (1994a), the other two time periods of high dissolved oxygen are the middle Eocene–early Oligocene and the middle Miocene–Holocene, each of which was preceded by low oxygen periods: Early Eocene and Late Oligocene. Therefore, the relationship between periods of formation of low and high levels of oxygen in bottom oceanic waters is not coincidental, but only during post-Turonian–Palaeocene times did such conditions result in widespread deposition of deep-sea oxic red clay and marl deposits (Hu, 2002; Hu et al., in press).

Conditions similar to those in southern Tibet developed in most of the western Tethys during the Late Cretaceous, as indicated by the occurrence of pelagic red beds in a discontinuous belt extending from the Exmouth Plateau in the east, across the Himalayas to the Caucasus, Carpathians, Alps and Apennines, the central North Atlantic, and the Caribbean (Hu et al., in press). The oxygenated waters not only influenced deep ocean basins, where deposition occurred below the CCD, but also extended up continental slopes, as indicated by red marls such as the Scaglia Rossa in Italy (Arthur and Fischer, 1977; Premoli Silva and Sliter, 1994), the Puchovske Marls in Slovakia (Michalik et al., 2002), the Kapanboğazi Formation in northern Turkey (Görür et al., 1993), and the Pustelnia and Macelowa marlstones in southern Poland (Bak, 1998). This suggests that not only the bottom waters but also the intermediate waters were highly oxygenated.

Upper Cretaceous oceanic red beds have their typical characters, especially compared with underlying mid-Cretaceous black shales (see Table 4). In this paper, we prefer to use the terminology OOE "Oceanic Oxic Event" to describe the change of sediment from mid-Cretaceous anoxic/dysoxic black shales to the younger oceanic red beds.

A final question is: What were the circumstances leading to the change from a dysoxic/anoxic deep-ocean bottom environment to an oxic environment in the Late Cretaceous? One hypothesis is that excess organic carbon burial during the mid-Cretaceous OAE may have affected CO_2 and O_2 concentrations in the oceans and atmosphere (Jenkyns, 1980; Arthur et al., 1988). A significant reduction in pCO_2 as a result of burial of a large amount of organic carbon during the mid-Cretaceous could have resulted in global climatic cooling (Spicer and Corfield, 1992; Voigt, 2000), which could have increased the vigour of thermohaline ocean-bottom circulation and, hence, the oxygen supplied to the deep-water environment.

Upper ocean water temperatures estimated from planktonic $\delta^{18}O$ data from well-preserved planktonic foraminifera suggest that surface water temperatures were highest during the Turonian in the western North

Table 4
Comparison of characteristics of the Late Cretaceous oceanic red beds and mid-Cretaceous black shales

	Colour	Lithology	Fossils	Lamination	Bioturbation	Pyrite
Oceanic red beds	Pink, red to maroon	From shale to limestone	Rich	No lamination	Common	No
Black Shales	Dark to black	Commonly shales	Few to rare	Laminated	Few to none	Rich
	Hematite	$\delta^{13}C$	TOC	Dissolved oxygen level at sediment-water surface	Distribution	Event
Oceanic red beds	Rich	? Negative	Very low	High	Global	OOE
Black Shales	No	Positive	High	Very low	Global	OAE

Atlantic (Norris et al., 2002; Wilson et al., 2002) followed by a slow cooling towards the end of the Cretaceous. However, in the South Atlantic warming continued up to the Campanian (Huber et al., 1995; Barrera and Savin, 1999; Stoll and Schrag, 2000). Hence, there is no straightforward relationship between climatic change and the change to an oxic deep-sea depositional environment because the development of an oxic environment in the southern Tethys would have occurred during a warming, not a cooling, period.

A major change in the thermohaline circulation of the oceans is the third potential factor for changing oxygen levels in deep water. During the Early Cretaceous, oceanic connections between the North and South Atlantic remained closed, preventing the flow of deep, oxygenated waters from polar areas to southern ocean basins (Philip et al., 1993; Wagner and Pletsch, 1999). The seaway between the North and South Atlantic most probably opened during the Albian, but deep oceanic circulation may not have been established until the Cenomanian or early Turonian (Hay et al., 1999; Pletsch et al., 2001). The development of pelagic red beds in the central North Atlantic and western Tethys therefore occurred prior to the opening of the equatorial seaway for deep oceanic circulation. It remains unproven whether the general oceanic circulation during the Cretaceous Period was similar to that of the present day or different. Some researchers have suggested that during the Late Cretaceous deep bottom water formed at low latitudes as warm, saline waters and flowed poleward (Hay, 1995; Hay and DeConto, 1999; Haupt and Seidov, 2001). According to this hypothesis, warm oxygen-rich bottom water could have been present in the central Tethyan Ocean during the Santonian–Campanian, which is the main depositional period of the oceanic red beds (Hu et al., in press).

Among other processes, the oxidized character of red deep-sea shales (except deposits on continental slopes) is associated with exceptionally low sedimentation rates. Examples are modern red clays in the Pacific that accumulate at a rate of less than 1 mm/ka (Glasby, 1991), and Upper Cretaceous red shales in the deep North Atlantic Basin that represent rates of 3–5 mm/ka (Jansa et al., 1979). The sedimentation rate, uncorrected for compaction, of red beds in southern Tibet is estimated to be 13 mm/ka. This is similar to the 8–13 mm/ka rate for the Scaglia Rossa in Italy (Arthur and Fischer, 1977), the 10 mm/ka rate of the Santo Ines section in Spain (Stoll and Schrag, 2000), and the 19.1 mm/ka rate of other Tethyan sections (Scott et al., 2004). The higher depositional rates for red beds in the Chuangde Formation are mainly a result of the incorporation of carbonate density-flow deposits. Rates of less than several mm/ka may not require a dramatic change in ocean-water chemistry to result in oxidation of sediments deposited below the CCD. However, because Tethyan red marlstones and limestones on continental slopes were also oxidized during this period, not only bottom waters but also intermediate waters were oxygenated; thus the oxic processes were not restricted to areas of low sedimentation rates.

6. Conclusions

Planktonic foraminifera and nannofossils indicate that the Chuangde Formation is Santonian–early Campanian in age, basically corresponding to zones CC15–17. The red shales in the formation represent deposition in an oceanic environment below the CCD; hence, they are deep-basin facies. The intercalated red marlstone beds represent recurring slumps from the upper slope or outer deep shelf into an adjacent deep basin. Sedimentation of the red facies took place in highly oxygenated bottom waters on the sea floor. This is confirmed by the red colour of the sediments, the high content of iron trioxide, the negative Cerium anomaly in the basal part of the succession, and the very low TOC content. The depositional regime in southern Tibet was similar to that in other areas of the western Tethys, such as the Apennines, Italy, where oxic waters impinged on the lower part of the continental slope, as indicated by the reddish coloured marls in the slumps. This indicates that not only the bottom waters but also the intermediate waters were highly oxygenated at the time of red bed deposition.

Several different processes or their combination may have been responsible for the environmental change from the deposition of dysoxic, dark grey facies to oxic, red beds. They include an excess of organic carbon burial, global climatic cooling, and/or intensification of bottom circulation. Also, a low sedimentation rate may have played an important role in the formation of the red beds. However, further studies are needed to understand the triggering mechanism. The site of deposition of the Chuangde Formation was near 20° S palaeolatitude, thus demonstrating that highly oxygenated bottom-water conditions were present in the southern Tethys as well as in the north.

Acknowledgements

We acknowledge the use of foraminiferal and nannofossil data provided by Wan Xiaoqiao (Chinese University of Geosciences, Beijing) and Maria Ovechkina (Russian Academy of Sciences, Moscow) respectively. We thank Luba Jansa, Hans Wielens and Elvira H. Gastaldo for their critical and helpful comments on an earlier draft of the manuscript. Prof. D.J. Batten is warmly thanked for improving our English. This work is supported by the NSFC Project (49625203, 40332020)

and MOST Pre-973 Project (2001CCA01800) to C. Wang, and a 1999 AAPG Grant-In-Aid to X. Hu. This is a contribution to IGCP projects 463 and 494.

References

Arthur, M.A., Dean, W., Pratt, L.M., 1988. Geochemical and climatic effects of increased marine organic carbon burial at the Cenomanian/Turonian boundary. Nature 335, 714–717.

Arthur, M.A., Fischer, A.G., 1977. Upper Cretaceous–Paleocene magnetic stratigraphy at Gubbio, Italy I. Lithostratigraphy and sedimentology. Geological Society of American, Bulletin 88, 367–371.

Bak, K., 1998. Planktonic foraminiferal biostratigraphy, Upper Cretaceous red pelagic deposits, Pieniny Klippen Belt, Carpathians. Studia Geologica Polonica 111 (13), 7–92.

Barrera, E., Savin, S.M., 1999. Evolution of late Campanian–Maastrichtian marine climates and oceans. In: Barrera, E., Johnson, C.C. (Eds.), Evolution of the Cretaceous Ocean-Climate System. Geological Society of America, Special Paper 332, pp. 245–282.

Burchfiel, B.C., Chen, Z.L., Hodges, K.V., Liu, Y.P., Royden, L.H., Changrong, D., Jiene, X., 1992. The South Tibetan detachment system, Himalayan orogen, extension contemporaneous with and parallel to shortening in a collisional mountain belt. Geological Society of America, Special Paper 269, 41 pp.

Caron, M., 1985. Cretaceous planktonic foraminifera. In: Bolli, H.M., Saunders, J.B., Perch-Nielsen, K. (Eds.), Plankton Stratigraphy. Cambridge University Press, Cambridge, pp. 17–86.

Colley, S., Wilson, T.R.S., Higgs, N.C., 1984. Post-depositional migration of elements during diagenesis in brown clay and turbidity sequences in the North East Atlantic. Geochimica Cosmochimica Acta 48, 1223–1235.

Erbacher, J., Thurow, J., 1997. Influence of oceanic anoxic events on the evolution of mid-Cretaceous radiolaria in the North Atlantic and western Tethys. Marine Micropaleontology 30, 139–158.

Eren, M., Kadir, S., 1999. Colour origin of upper Cretaceous pelagic red sediments within the Eastern Pontides, northeast Turkey. International Journal of Earth Science 88, 593–595.

Gansser, A., 1964. Geology of the Himalayas. Wiley Interscience, London, 289 pp.

Glasby, G.P., 1991. Mineralogy, geochemistry, and origin of Pacific red clays: a review. New Zealand Journal of Geology and Geophysics 34, 167–176.

Görür, N., Tuysuz, O., Aykol, A., Sakinc, M., Yigitbas, E., Akkok, R., 1993. Cretaceous red pelagic carbonates of northern Turkey; their place in the opening history of the Black Sea. Eclogae Geologicae Helvetiae 86, 819–838.

Hardenbol, J., Thierry, J., Farley, M.B., Jacquin, T., de Graciansky, P.C., Vail, P.R., 1998. Mesozoic and Cenozoic sequence chronostratigraphic framework of European basins. In: de Graciansky, P.C., Hardenbol, J., Jacquin, T., Vail, P.R. (Eds.), Mesozoic and Cenozoic Sequence Stratigraphy of European Basins. SEPM (Society for Sedimentary Geology) Special Publication 60, pp. 3–13.

Harries, P.J., 1999. Repopulation from Cretaceous mass extinctions: environmental and/or evolutionary controls? In: Barrera, E., Johnson, C.C. (Eds.), Evolution of the Cretaceous Ocean-Climate System. Geological Society of America, Special Paper 332, pp. 345–364.

Harries, P.J., Kauffman, E.G., Hansen, T.A., 1996. Models for biotic survival following mass extinction. In: Hart, M.B. (Ed.), Biotic Recovery from Mass Extinction Events. Geological Society, London, Special Publication 102, pp. 41–60.

Haupt, B.J., Seidov, D., 2001. Warm deep-water ocean conveyor during Cretaceous time. Geology 29, 295–298.

Hay, W.W., 1995. Cretaceous paleoceanography. Geologica Carpathica 46, 257–266.

Hay, W.W., DeConto, R.M., 1999. Comparison of modern and Late Cretaceous meridional energy transport and oceanology. In: Barrera, E., Johnson, C.C. (Eds.), Evolution of the Cretaceous Ocean-Climate System. Geological Society of America, Special Paper 332, pp. 283–300.

Hay, W.W., DeConto, R.M., Wold, C.N., Wilson, K.M., Voigt, S., Schulz, M., Wold-Rossby, A., Dulb, W.C., Ronov, A.B., Balukhovsky, A.N., Soeding, E., 1999. Alternative global Cretaceous paleogeography. In: Barrera, E., Johnson, C.C. (Eds.), Evolution of the Cretaceous Ocean-Climate System. Geological Society of America, Special Paper 332, pp. 1–47.

Holser, W.T., 1997. Evaluation of the application of rare-earth elements to paleoceanography. Palaeogeography, Palaeoclimatology, Palaeoecology 132, 309–323.

Hu, X.M., 2002. Sedimentary geology of Cretaceous in southern Tibet, and the Upper Cretaceous oceanic red beds. Unpublished PhD Thesis, Chengdu University of Technology, 216 pp.

Hu, X.M., Wang, C.S., Li, X.H., 2001. The stable carbon isotope of Cretaceous carbonate and its response to paleo-ocean dissolved-oxygen events in southern Tibet. Progress in Natural Science 10, 341–349.

Hu, X.M., Jansa, L., Wang, C.S., Sarti, M., Bak, K., Wagreich, M., Michalik, J., Soták, J., 2005. Upper Cretaceous Oceanic Red Beds (CORBs) in the Tethys: occurrences, lithofacies, age, and environments. Cretaceous Research, 26, this issue.

Huber, B.T., Hodell, D.A., Hamilton, C.P., 1995. Middle–Late Cretaceous climate of the southern high latitudes: stable isotopic evidence for minimal equator-to-pole thermal gradients. Geological Society of America, Bulletin 107, 1164–1191.

Jansa, L.F., Enos, P., Tucholke, B.E., Gradstein, F.M., Sheridan, R.E., 1979. Mesozoic–Cenozoic sedimentary formations of the North American Basin, western North Atlantic. In: Talwani, M., Hay, W., Ryan, W.B.F. (Eds.), Deep Drilling Results in the Atlantic Ocean. Continental Margins and Paleoenvironment. American Geophysical Union, Maurice Ewing Series 3, pp. 1–57.

Jenkyns, H.C., 1980. Cretaceous anoxic events: from continents to oceans. Journal of the Geological Society, London 137, 171–188.

Jenkyns, H.C., Gale, A.S., Corfield, R.M., 1994. Carbon and oxygen isotope stratigraphy of the English Chalk and Italian Scaglia and its paleoclimatic significance. Geological Magazine 131, 1–34.

Kaiho, K., 1994a. Planktonic and benthic foraminiferal extinction events during the last 100 m.y. Palaeogeography, Palaeoclimatology, Palaeoecology 111, 45–71.

Kaiho, K., 1994b. Benthic foraminiferal dissolved-oxygen index and dissolved-oxygen levels in the modern ocean. Geology 22, 719–722.

Krenmayr, H.G., 1996. Hemipelagic and turbiditic mudstone facies associations in the Upper Cretaceous Gosau Group of the Northern Calcareous Alps (Austria). Sedimentary Geology 101, 149–172.

Leckie, R.M., Bralower, T.J., Cashman, R., 2002. Oceanic anoxic events and plankton evolution: biotic response to tectonic forcing during the mid-Cretaceous. Paleoceanography 17 (3), doi: 10.1029/2001PA000623.

Li, X.H., Wang, C.S., Wan, X.Q., Tao, R., 1999. Verification of stratigraphic sequence and classification for the Chuangde cross-locality of Gyangze, southern Tibet. Journal of Stratigraphy 23, 303–309 (in Chinese, English abstract).

Liu, G., Einsele, G., 1994. Sedimentary history of the Tethyan Basin in the Tibetan Himalayas. Geologische Rundschau 83, 32–61.

Liu, G., Einsele, G., 1996. Various types of olistostromes in a closing ocean basin, Tethyan Himalaya (Cretaceous, Tibet). Sedimentary Geology 104, 203–226.

Liu, J.B., Aitchison, J.C., 2002. Upper Paleocene radiolarians from the Yamdrok mélange, south Xizang (Tibet), China. Micropaleontology 48 (Suppl. 1), 145–154.

Liu, Y.G., Miah, M.R.U., Schmitt, R.A., 1988. Cerium: a chemical tracer for paleo-oceanic redox conditions. Geochimica Cosmochimica Acta 52, 1361–1371.

Michalik, J., Soták, J., Salaj, J., 2002. Cretaceous Oceanic Red Beds in the westernmost Carpathians in Slovakia. In: Hu, X., Sarti, M. (Eds.), Cretaceous Oceanic Red Beds (CORB) in an Apennines-Alps-Carpathians Transect, Field Guidebook for Inaugural Workshop of IGCP 463, Ancona, Italy, pp. 47–72.

Morford, J.L., Emerson, S., 1999. The geochemistry of redox sensitive trace metals in sediments. Geochimica Cosmochimica Acta 63, 1735–1750.

Morford, J.L., Russell, A.D., Emerson, S., 2001. Trace metal evidence for changes in the redox environment associated with the transition from terrigenous clay to diatomaceous sediment, Saanich Inlet, BC. Marine Geology 174, 355–369.

Norris, R.D., Bice, K.L., Magno, E.A., Wilson, P.A., 2002. Jiggling the tropical thermostat during the Cretaceous hot house. Geology 30, 299–302.

Patzelt, A., Li, H., Wang, J., Appel, E., 1996. Palaeomagnetism of Cretaceous to Tertiary sediments from southern Tibet, evidence for the extent of the northern margin of India prior the collision with Eurasia. Tectonophysics 259, 259–284.

Perch-Nielsen, K., 1985. Mesozoic calcareous nannofossils. In: Bolli, H.M., Saunders, J.B., Perch-Nielsen, K. (Eds.), Plankton Stratigraphy. Cambridge University Press, Cambridge, pp. 329–426.

Philip, J., Babinot, J.F., Tronchetti, G., Fourcade, E., et al. (7 others), 1993. Late Cenomanian (94–92 Ma). In: Dercourt, J., Ricou, L.E., Vrielynck, B. (Eds.), Atlas of Tethys Paleoenvironmental Maps. Gauthier-Villars, Paris, pp. 153–178.

Piper, D.Z., 1974. Rare earth elements in the sedimentary cycle: a summary. Chemical Geology 14, 285–304.

Piper, D.Z., 1994. Seawater as the source of minor elements in black shales, phosphorites and other sedimentary rocks. Chemical Geology 114, 95–114.

Pletsch, T., Erbacher, J., Holbourne, A.E.L., Kuhnt, W., Moullade, M., Oboh-Ikuenobe, F.E., Söding, E., Wagner, T., 2001. Cretaceous separation of Africa and South America: the view from the West African margin (ODP Leg 159). Journal of South American Earth Sciences 14, 147–174.

Premoli Silva, I., Sliter, W.V., 1994. Cretaceous planktonic foraminiferal biostratigraphy and evolutionary trends from the Bottacione section, Gubbio, Italy. Paleontologia Italica 82, 1–89.

Raup, D.M., Sepkoski Jr., J.J., 1984. Periodic extinctions of families and genera. Science 231, 833–836.

Robaszynski, F., Caron, M., 1995. Foraminifères planctoniques du Crétacé: commentaire de la zonation Europe-Méditerranée. Bulletin de la Société Géologique de France 166, 681–692.

Schlanger, S.O., Arthur, M.A., Jenkyns, H.C., Scholle, P.A., 1987. The Cenomanian–Turonian oceanic anoxic event; I, stratigraphy and distribution of organic carbon-rich beds and the marine: $\delta^{13}C$ excursion. In: Brooks, J., Fleet, A.J. (Eds.), Marine Petroleum Source Rocks. Geological Society, London, Special Publication 26, pp. 371–379.

Schlanger, S.O., Jenkyns, H.C., 1976. Cretaceous oceanic anoxic events: cause and consequence. Geologie en Mijnbouw 55, 179–184.

Scholle, P.A., Arthur, M.A., 1980. Carbon isotope fluctuations in Cretaceous pelagic limestones: potential stratigraphic and petroleum exploration tool. American Association of Petroleum Geologists, Bulletin 64, 67–87.

Scott, R.W., Hu, X.M., Malata, E., Melinte, M., Sanders, D., Shcherbinina, E.A., Skupien, P., Wagreich, M., 2004. Timing and rates of deposition of Cretaceous oceanic red beds. 32nd International Geological Congress, Abstracts, Part 1, p. 573.

Shimizu, H., Masuda, K., 1977. Cerium in chert as an indication of marine environment of its formation. Nature 266, 346–348.

Spicer, R.A., Corfield, R.M., 1992. A review of terrestrial and marine climates in the Cretaceous with implications for modelling the "Greenhouse Earth". Geological Magazine 129, 169–180.

Stoll, H.M., Schrag, D.P., 2000. High-resolution stable records from the Upper Cretaceous rocks of Italy and Spain: glacial episodes in a greenhouse planet? Geological Society of America, Bulletin 112, 308–319.

Thomson, J., Colley, S., Higgs, N.C., Hydes, D.J., Wilson, T.R.S., Sorensen, J., 1987. Geochemical oxidation trends in NE Atlantic distal turbidites and their effects in the sedimentary record. In: Weaver, P.P.E., Thomson, J. (Eds.), Geology and Geochemistry of Abyssal Plains. Geological Society, London, Special Publication 31, pp. 167–177.

Voigt, S., 2000. Cenomanian–Turonian composite $\delta^{13}C$ curve for Western and Central Europe: the role of organic and inorganic carbon fluxes. Palaeogeography, Palaeoclimatology, Palaeoecology 160, 91–104.

Wagner, T., Pletsch, T., 1999. Tectono-sedimentary controls on black shale deposition along the opening Equatorial Atlantic Gateway (ODP Leg 159). In: Cameron, N. (Ed.), Oil and Gas Habitats of the South Atlantic. Geological Society, London, Special Publication 153, pp. 241–265.

Wan, X.Q., Lamolda, M.A., Si, J.L., Li, G.B., 2005. Foraminiferal stratigraphy of Cretaceous red beds in southern Tibet. Cretaceous Research, 26, this issue.

Wang, C.S., Li, X., Wan, X., Tao, R., 2000. The Cretaceous in Gyangze, southern Tibet. Acta Geologica Sinica 74, 97–107 (in Chinese English abstract).

Wang, C.S., Hu, X.M., Jansa, L., Wan, X.Q., Tao, R., 2001. The Cenomanian–Turonian anoxic event in South Tibet. Cretaceous Research 22, 481–490.

Wang, C.S., Xia, D.X., Zou, X., Chen, J.P., 1996. Field Trip Guide T121/T387, Geology between the Indus-Yarlung Zangbo Suture Zone and the Himalaya Mountains (Xizang), China. Geological Publishing House, Beijing, 72 pp.

Willems, H., 1993. Sedimentary history of the Tibetan Tethys Himalaya continental shelf in South Tibet (Gamba, Tingri) during Upper Cretaceous and Lower Tertiary (Xizang Autonomous Region, PR China). In: Willems, H. (Ed.), Geoscientific Investigation in the Tethyan Himalayas. Berichte der Fachbereich Geowissenschaften, Universität Bremen 38, pp. 49–183.

Willems, H., Zhou, Z., Zhang, B., Grafe, K.U., 1996. Stratigraphy of the Upper Cretaceous and Lower Tertiary strata in the Tethyan Himalayas of Tibet (Tingri area, China). Geologische Rundschau 85, 723–754.

Wilson, P.A., Norris, R.D., Cooper, M.J., 2002. Testing the mid-Cretaceous greenhouse hypothesis using "glassy" foraminiferal calcite from the core of the Turonian tropics on Demerara Rise. Geology 30, 607–610.

Wilson, T.R.S., Thomson, J., Colley, S., Hydes, D.J., Higgs, N.C., Sorensen, J., 1985. Early organic diagenesis; the significance of progressive subsurface oxidation fronts in pelagic sediments. Geochimica Cosmochimica Acta 49, 811–822.

Yu, G., Wang, C., 1990. Sedimentary geology of the Xizang (Tibet) Tethys. Geological Memoir, Series 3, 12, Geological Publishing House, Beijing, 187 pp. (in Chinese, English abstract).